Time-dependent Marangoni-Bénard instability of an evaporating binary-liquid layer including gas transients

H. Machrafi,[1, a)] A. Rednikov,[2] P. Colinet,[2] and PC. Dauby[1]

[1)] *Université de Liège, Institut de Physique B5a, Allée du 6 Août 17, B-4000 Liège 1, Belgium*

[2)] *Université Libre de Bruxelles, TIPs - Fluid Physics, CP165/67, Avenue F.D. Roosevelt, 50, B-1050 Bruxelles, Belgium*

We are here concerned with Bénard instabilities in a horizontal layer of a binary liquid, considering as a working example the case of an aqueous solution of ethanol with a mass fraction of 0.1. Both the solvent and the solute evaporate into air (the latter being insoluble in the liquid). The system is externally constrained by imposing fixed "ambient" pressure, humidity and temperature values at a certain effective transfer distance above the liquid-gas interface, while the ambient temperature is also imposed at the impermeable rigid bottom of the liquid layer. Fully transient and horizontally homogeneous solutions for the reference state, resulting from an instantaneous exposure of the liquid layer to ambient air, are first calculated. Then, the linear stability of these solutions is studied using the frozen-time approach, leading to critical (monotonic marginal stability) curves in the parameter plane spanned by the liquid layer thickness and the elapsed time after initial contact. This is achieved for different ratios of the liquid and gas thicknesses, and in particular yields critical times after which instability sets in (for given thicknesses of both phases). Conversely, the analysis also predicts a critical thickness of the liquid layer below which no instability ever occurs. The nature of such critical thickness is explained in details in terms of transient mass fraction profiles in both phases, as it indeed appears that the most important mechanism for instability onset is the solutal Marangoni one. Importantly, besides the result obtained previously under the quasi-steady assumption in the gas phase [Machrafi *et al*, Eur. Phys. J. Special Topics **192**, 71 (2011)], it is shown that relaxing this assumption may yield essentially lower values of the critical liquid thickness, especially for large gas-to-liquid thickness ratios. A good-working analytical model is developed for the description of such delicate transient effects in the gas. The analysis reveals that the system considered in this paper is generally highly unstable, the instability setting in even for very small times and liquid thicknesses.

[a)]Electronic mail: H.Machrafi@ulg.ac.be

I. INTRODUCTION

In general, Bénard instabilities in horizontal liquid layers are those associated with imposed vertical temperature or concentration gradients[1−4]. The system is destabilized by means of the buoyancy and/or surface-tension-gradient mechanisms, the corresponding instabilities being named, respectively, Rayleigh-Bénard or Marangoni-Bénard. They are said to be thermal if caused by temperature gradients and solutal if caused primarily by concentration gradients. Moreover, it is also possible that the temperature gradients cause a solutal effect (the Soret effect) or that concentration gradients cause a thermal effect (the Dufour effect), even though the latter is typically considered negligible in the context of Bénard layers.

In the case of evaporating liquid layers, vertical temperature gradients occur naturally inside the system (even in isothermal surroundings) due to an evaporation-induced cooling of the interface. For binary mixtures, concentration gradients generally also occur due to different volatilities of the components. In short, evaporation is potentially able to induce both thermal and solutal Rayleigh-Marangoni-Bénard instabilities. The case of one-component liquids has been studied rather thoroughly in the literature (e.g. the papers[5,6], to mention a few). However, fewer studies exist as far as the case of two-component liquids is concerned. In the case the liquid is evaporating into its vapor, one can mention some works[7,8], where the importance of sidewall effects, surface deflection and of an imposed temperature gradient was analyzed. For the case the liquid is evaporating into an inert gas (which is of interest in the present paper), one can mention a theoretical study for a droplet with thermal and/or solutal Marangoni effects[9], a scaling analysis[10] for the solutal Bénard-Marangoni instability, studies of thermal and solutal Bénard problems on evaporating polymer solutions[11−13], an analysis of buoyancy-driven solutal instabilities in water-alcohol mixtures[14] and experiments were also reported[14−17]. Besides, the Bénard problem for an evaporating binary-mixture layer (10 %wt ethanol in water as a concrete example) was considered in our previous works[18,19] using quite a detailed physical model that includes the thermal and solutal Rayleigh and Marangoni effects, the Soret effect, and accounts for an active role of the gas phase (without merely describing using heat and mass transfer coefficients). The focus was on the critical liquid-layer thicknesses for the onset of monotonic instability. In[18], stability of quasi-stationary reference states was analyzed. Comparing the Marangoni and Rayleigh,

thermal and solutal effects with one another, it has been shown that the Marangoni effect is much more important than the Rayleigh effect and that the solutal effect is also by far more important than the thermal effect at least as far as the instability onset is concerned (for the system treated in this paper). The instability mechanism at the onset was thus concluded to be primarily of the solutal Marangoni type. Given the extremely small critical liquid layer thicknesses obtained in our analysis[18], we have also deduced that an initially well mixed binary liquid with a realistic thickness of, say, 1 mm should become unstable very shortly after its exposure to air, much before the transient diffusional boundary layers developing from the interface have reached the bottom of the liquid. This was confirmed in[19] by considering transient concentration reference profiles in the liquid, even though the other reference profiles were still considered as quasi-stationary. However, on the other hand, the small critical thickness values previously obtained[18,19] signal that the time scales associated in the instability development may be so small (i.e., fast) that the partial relaxation of the quasi-stationarity assumption adopted in[19] may not be overall sufficient. In particular, it would be interesting to examine if and when the transient behaviour in the gas phase should be taken into account in modeling the evaporation system of a binary mixture in contact with air. Thus, studying the instability with time-dependent reference profiles for both the temperature and the concentration in both the liquid and the gas layers is in principle of essential interest here. It is this kind of analysis that will be carried out in the present paper by means of the frozen-time approach, the focus being on both the critical time for instability onset (for given thicknesses of both layers) and on the critical thickness of the liquid layer (for a given ratio gas/liquid) below which no instability ever occurs. Nevertheless, as in the majority of works in the literature, we here still rely upon the quasi-stationary assumption as far as the variation of the liquid-layer thickness due to evaporation is concerned, in the sense that this variation is considered slow as compared to the diffusive and/or thermal time scales of the system. This essentially means that the thickness is assumed to remain effectively constant on the relevant time scales of the problem. In general, the influence of the ratio of the gas thickness to that of the liquid is then expected to play an important role. A parametric study will be carried out here for a number of gas/liquid thicknesses ratios. A significant departure from the results of[19] is actually expected first of all when these ratios are high, as will be detailed in this work.

The paper is organized as follows. First, the formulation is given in section II, describing

the physics of the problem. Then, the general results of the reference-state behavior and the stability analysis are presented in section III. Subsequently, these results are discussed, focusing on the predominant instability onset mechanism and on inessential effects (section IV.A), on the behavior at relatively small gas-to-liquid thickness ratios (section IV.B), and at relatively large ones (section IV.C), for which the importance of transients in the gas phase is identified (section IV.D). Conclusions are summarized in section V. Note that most technical details and mathematical developments, largely similar to those presented in[18] are presented in appendices A-E, which are provided as supplementary material[20]. The full mathematical description of the system is provided in appendix A, whereas appendices B and C describe its application to the reference state and to the problem for perturbations, respectively. Appendix D is dedicated to an approximate, Pearson-like model, widely used in the discussion of section IV. Finally, appendix E considers the small-time limit of this latter model, which is also widely referred to in sections III and IV. The present paper has been written, however, in order to be understandable without necessarily consulting this supplementary material.

II. FORMULATION

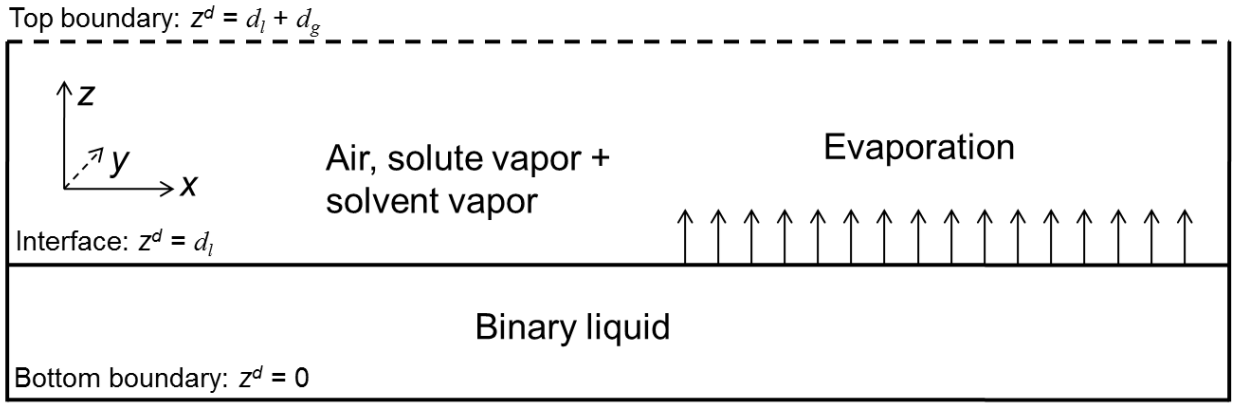

FIG. 1. Sketch of the system.

A sketch of the physical system is presented in Fig. 1. It consists of a horizontal binary (solvent and solute) liquid layer of thickness d_l evaporating into an inert gas through an undeformable interface. A discussion on the justification of assuming an undeformable interface can be found in previous work[18] and applies here as well, since we are here interested

in non-longwave modes of instability, for which the surface deformability is well suppressed by the capillarity (cf.[18]). Inert-gas absorption into the liquid is neglected. The gas layer thickness is here given by a certain "transfer distance", d_g. It can be described as a typical equivalent (effective) diffusion length in the gas phase at which the diffusive transport is formally of the same magnitude as the convective transport in a real setup, as determined by air currents which may be naturally present (e.g. due to buoyancy) or deliberately created (ventilation). In this approach, the gas located above the gas layer, of thickness d_g, is considered as perfectly mixed while ensuring given "ambient" values of temperature and mass fractions (humidity) at the effective upper boundary of the gas layer. The total pressure is also imposed there. More details on such an approach are given in[5,18]. Other boundary conditions imposed at the top of the gas phase are a constant normal stress and a zero shear stress[18]. At the liquid-gas interface, the following conditions are considered: the tangential stress balance including the thermal and solutal Marangoni stresses, the no-slip condition, the temperature continuity, the heat flux balance including the heat of evaporation, the mass flux conservation (for each species) and the local equilibrium (Henry's law for the solute and Raoult's law for the solvent, assuming a sufficiently dilute case). At the bottom of the liquid layer we consider a constant temperature T_b (the same as at the top of the gas layer), the index "b" formally indicating the bottom boundary (even though T_b is actually the ambient temperature here), the no-slip condition and a zero normal velocity. As for the mass fraction condition at the bottom, it is governed by a zero-flux condition, expressing that the bottom boundary is impermeable. The Boussinesq approximation is adopted for both phases of the system, implying that the material properties of the fluids are treated as constant except for the density in the buoyancy terms, where it depends linearly on the temperature and mass fractions. In full, the equations and boundary conditions are provided in appendix A1. This model is in fact quite similar to the one used previously[18,19] and for this reason a step-by-step development of the equations is not repeated here in the main text.

Initially, the liquid is at rest ($\vec{v}_l = 0$, with $\vec{v}$ the barycentric velocity), with an initial temperature $T_l = T_b$ and an initial mass fraction $c_l = c_b$. The gas has an initial temperature $T_g = T_b$ and initial solvent and solute vapor mass fractions $c_{g1} = c_{t1}$ and $c_{g2} = c_{t2}$. The subscripts "l" and "g" relate to the liquid and gas phases, respectively. The subscripts "1" and "2" stand for the solvent and the solute, respectively. The subscript "t" refers to the top boundary (of the gas layer), and thus c_{t1} and c_{t2} actually correspond to the ambient humidity

expressed in terms of the mass fractions. Let us define the moments before evaporation is allowed as $t < 0$ and the time it is enabled as $t = 0$. From $t = 0^+$ on, the time-evolving temperature and mass fraction profiles in the liquid and gas phases start to develop in the form of boundary layers growing from the interface. After a certain time, this transient state may become unstable and this instability is the main question analyzed in the present paper. In the present analysis, the liquid will be a mixture of water (solvent) and ethanol (solute). The inert gas is air. We shall also choose $T_b = 300K$, $c_b = 0.1$, $c_{t1} = 0$ and $c_{t2} = 0$. The physical properties used in this paper can be found in Table I of appendix A3. The references to the sources of these physical properties can be found in previous work[18]. Note that we have chosen here a zero humidity for the air far from the interface, with zero concentrations for both solvent and solute ($c_{t1} = 0$ and $c_{t2} = 0$). Should water evaporate slower, due to a larger humidity in the gas, the concentration gradients in the liquid become stronger, obtaining a more unstable system. In the present paper, we have chosen not to make a parametric study versus the humidity, focusing on other pertinent issues.

First, one has to determine the horizontally uniform reference state of which the stability will be analyzed later on. The corresponding formulation is easily deduced from the general one. Certain details are provided in appendix B. In the present work, the problem for the reference state is solved numerically, using a standard finite-difference method.

Then, small perturbations are superimposed over the reference solution and their evolution is studied. The linearized formulation for perturbations is given in appendix C. It is here obtained under the so-called frozen-time approach, which consists in carrying out the stability analysis of the reference solution at a certain instant as if this reference solution were stationary, as previously used[18,19,21]. Therefore, normal modes are introduced and the growth rates σ of these modes are calculated by solving an eigenvalue problem, using a spectral Tau-Chebyshev method (a classical spectral method that is described in the literature[18,22–26] and explained in[27]). The marginal condition is then determined by $\sigma = 0$ (here it turns out that the eigenvalues σ are all real and thus the instability is always monotonic).

Chosen the solute, solvent and inert gas and given the ambient conditions, the main control parameters we are left with are d_l and d_g or, equivalently, d_l and $H \equiv (d_l + d_g)/d_l$. In the present paper, we consider H as a fixed parameter and for a given dimensionless time t (and the corresponding instantaneous reference profiles), we calculate the critical

liquid thickness d_l corresponding to $\sigma = 0$. The results (for a fixed H) can also be (more intuitively) interpreted inversely by plotting the critical time t at which a layer of a given thickness d_l possesses a marginal frozen-time perturbation.

III. RESULTS

We present here the general results of our work. First, the evolution of the reference solution is described and some of its characteristics are emphasized for later use. Then, the results of the linear stability analysis are considered. Further discussion and details will be provided in section IV.

A. Reference state

When evaporation starts at $t = 0$, the evolution of the reference solution consists first and foremost in the development of five diffusive boundary layers in the originally spatially uniform liquid and gas layers: the temperature T_l and solute mass fraction c_l in the liquid phase ($1 - c_l$ is then that of the solute) and the temperature T_g as well as the solute and solvent mass fractions c_{g1} and c_{g2} in the gas phase ($1 - c_{g1} - c_{g2}$ is then that of air). The development of these boundary layers is also accompanied by a decrease of the liquid thickness due to evaporation, but the latter is assumed to be very slow at the relevant time scales here, and hence the thickness variation is neglected (or, in other words, treated quasi-stationarily). Later on in this paper, we will also show that the reference profiles of the temperature field do not play a significant role. For all these reasons, our comments in the present section will mainly focus on the mass fraction reference profiles in the gas and liquid phases.

Fig. 2 shows the time evolution of the reference profiles for the solute mass fraction in the liquid and for the solute and solvent mass fractions in the gas for three values of the parameter H. The time variable is here dimensionless, the scale being d_l^2/D_l, where D_l is the diffusion coefficient in the liquid. As a first observation, let us stress that the mass fractions on both sides of the liquid-gas interface present a certain instantaneous "jump" at $t = 0$, a consequence of suddenly bringing into contact two uniform media that are not in equilibrium with each other. For whatever H value, the interface values suddenly jump

to $c_l \approx 0.0979$, $c_{g1} \approx 0.0210$ and $c_{g2} \approx 0.0211$ from the initial values $c_l = 0.1$, $c_{g1} = 0$ and $c_{g2} = 0$, respectively. The jump and the development of the boundary layers at these small times can actually be described by standard self-similar solutions (appendix E), for which the mass fractions at the interface remain constant. After some time, these boundary layers will however reach the limits of the system and the self-similar description loses its validity (hence leading to a departure from the interfacial values of c_l, c_{g1} and c_{g2} just mentioned as seen in Fig. 2). Depending on the value of parameter H, either the liquid boundary layers will first attain the bottom (sufficiently large H) or the gas boundary layers will first attain the top (sufficiently small H), or both simultaneously (in some intermediate range of H).

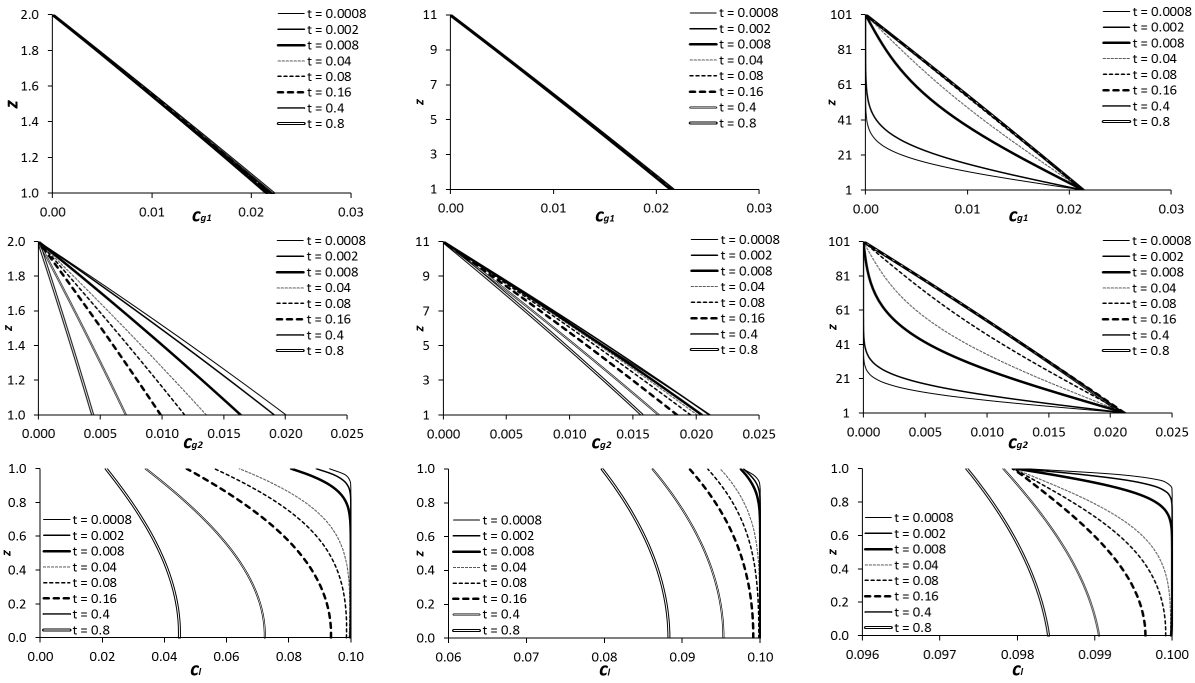

FIG. 2. The reference solution for the solvent mass fraction in the gas (upper), the solute mass fraction in the gas (intermediate) and the solute mass fraction in the liquid (lower) for $H = 2$ (left), 11 (middle) and 101 (right) at an initial mass fraction of $c_b = 0.1$ in the liquid and $c_{t1} = c_{t2} = 0$ in the gas, for several dimensionless times.

Let us speak first in further detail about the gas boundary layers. After they have reached the top of the system, where the mass fractions are assumed to be fixed, the corresponding profile becomes almost linear (in view of a small Péclet number of the Stefan flow in the gas, justifying its neglecting[18]) with respect to the vertical coordinate, with a slope of this profile, and hence a mass flux, being determined by the values of the mass fraction at the interface

and at the top of the layer. The term "quasi-stationary" is appropriate to characterize the corresponding evolution in the gas, driven by an active evolution in the liquid phase. In general, a model involving transient reference profiles in the liquid but yet quasi-stationary ones in the gas (irrespective of whether the latter is justified or not) will be here referred to as partially transient[19]. Since the ethanol boundary layer in the gas phase attains the top boundary later than the water boundary layer ($D_{g1} > D_{g2}$), the quasi-stationarity character in the gas is to be assessed by the ethanol vapor distribution. A certain time can thus be defined that distinguishes the self-similar stage (sufficiently below this time) from the quasi-stationary state (sufficiently above this time). It scales in the gas with the typical diffusion time d_g^2/D_{g2} in dimensional terms and $\delta_D^{-1}(H-1)^2$ in dimensionless terms (non-dimensionalized with the diffusion time d_l^2/D_l in the liquid). Similarly, the time for the liquid boundary layer to reach the bottom scales as d_l^2/D_l in dimensional terms and as $O(1)$ in dimensionless terms.

The self-similar solution takes place for t sufficiently smaller than both these times and is first violated from the gas side for relatively small H, and from the liquid side for relatively large H. These considerations are of interest when discussing the evolution of the overall mass fraction difference across the liquid layer, which plays an important role in the instability development, as seen later. This quantity is plotted in Fig. 3 for various H values.

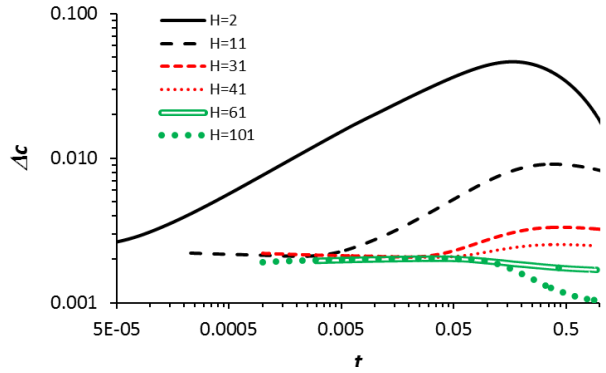

FIG. 3. The overall mass fraction difference $\Delta c = c_b - c_{i,ref,l}$ across the liquid layer versus the dimensionless time for a number of H values and an initial mass fraction of $c_b = 0.1$ in the liquid and $c_{t1} = c_{t2} = 0$ in the gas.

As a first observation of Fig. 3, we note that for all H, the mass fraction difference tends

to a unique constant value for t going to 0. This value is determined by the initial "jump" described above and is given by $\Delta c = c_b - c_{i,ref,l} \approx 0.0021$. Secondly, Fig. 3 manifests a small initial time period where the mass fraction difference across the liquid layer remains nearly constant. This period corresponds to the self-similar evolution. Note also that the left side of this "plateau" is not perfectly flat due to numerical difficulties at the beginning of the calculation resulting from the discontinuous initial jump. Just after the initial plateau, it is important to note that a certain maximum mass fraction difference across the liquid layer occurs for sufficiently small values of H. Note that for these H values, the gas reaches quasi-stationarity before the liquid boundary layer reaches the bottom. After the gas mass fraction profiles have become quasi-stationary, the self-similar solution is not valid anymore and the ethanol flux in the gas stops its fast $t^{-1/2}$ decrease (characterizing the self-similar solution) to saturate to some quasi-constant value. The liquid layer is then progressively not able to supply ethanol sufficiently fast anymore, which depletes ethanol at the interface and thus increases the mass fraction difference in question. This increase reverses when the liquid boundary layer reaches the bottom of the system and the ethanol depletion starts to occur at the bottom as well. The time corresponding to the maximum mass fraction difference, $t_{\Delta c,max}$, is given as a function of H in Table I. The inevitability of such a reversal can readily be understood from the consideration that, for any H, the overall mass fraction difference must tend to zero at large times, due to the progressive depletion of ethanol. Of course, this entails also a diminution of the liquid layer thickness, which is neglected in this study and therefore it is not consistent to pursue the calculations up to such advanced stages of the process. It is also important to stress that this maximum actually exists for $H < 46$ only, meaning that, for higher H values, the depletion of ethanol from the bottom starts relatively earlier than a sufficient degree of quasi-stationarity is attained in the gas.

B. Global results of the stability analysis

As explained previously, for a fixed H and at a given instant of time t (corresponding to given "frozen" reference profiles), the stability analysis as carried out here consists in calculating the critical liquid depth above which the layer is unstable (in the frozen-time sense). This actually turns out to be equivalent to determining the critical time at which a layer of a given thickness d_l changes its stability status, as illustrated in Fig. 4, which

TABLE I. Several dimensionless (scale d_l^2/D_l) characteristic times for different H values. Namely, $t_{\Delta c,max}$ for the maximum overall mass fraction difference across the liquid layer; t_{TP1} for the turning point of the first type and t_{TP2} for the turning point of the second type, see also section III B. For n/a entries, the corresponding values cannot be defined.

H	2	11	21	31	41	46	49	50	51	52	53	56	61	101
$t_{\Delta c,max}$	0.17	0.39	0.42	0.44	0.44	0.51	0^+	0^+	0^+	0^+	0^+	0^+	0^+	0^+
t_{TP1}	0.16	0.37	0.4	0.4	0.4	0.15	n/a	n/a	n/a	n/a	n/a	n/a	n/a	n/a
t_{TP2}	n/a	n/a	n/a	n/a	n/a	0.03	0.03	0.03	0.03	0.03	0.03	0.03	0.03	0.03

presents the general results of our work. Here, the results are presented in terms of both dimensional and dimensionless times. The dimensionless time used on the left plot of Fig. 4 allows relating the instability thresholds with the corresponding reference profiles (i.e. for a given liquid thickness) in Fig. 2. Since we will proceed with dimensional times, the general results are also presented with dimensional times on the right plot of Fig. 4. We continue with the critical curves (marginal stability) that are plotted in the plane spanned by the (dimensional) time t and the liquid thickness d_l for different H values. We notice that for all H, a minimum critical liquid depth exists below which no instability ever occurs. This minimum value is determined by what we shall call the turning point (TP) of the corresponding curve and the value of the liquid depth at this point will be denoted as $d_{l,TP}$. Thus the present evaporative Bénard-Marangoni instability must not occur in liquid layers with depths $d_l < d_{l,TP}$, whatever the time elapsed. The TP can also be considered as a separatrix between the "upper" and "lower" parts of each curve. For a given $d_l > d_{l,TP}$, the lower part of the curve gives the critical time at which perturbations to the frozen-time profile begin to grow. These perturbations start to decay once again at t corresponding to the upper branch, of course, unless the instability setting in at shorter times has had enough time to develop into a manifest convection considerably altering the reference state. It is also interesting to emphasize that the position of the TP changes with H, at least for sufficiently small values of H. For H around 41, a second TP actually emerges on the critical curve. This second TP appears to be largely independent of H at $H > 41$, while the first one progressively disappears as H is increased above $H > 41$. Note also that the lower parts of the different curves tend to one another for increasing values of the liquid

thickness d_l. This is not clearly visible for $H = 2$ due to numerical difficulties. However, using an approximate solution of the complete model, we show later on in Fig. 9 that the curve $H = 2$ joins indeed the other curves as well when d_l is increased.

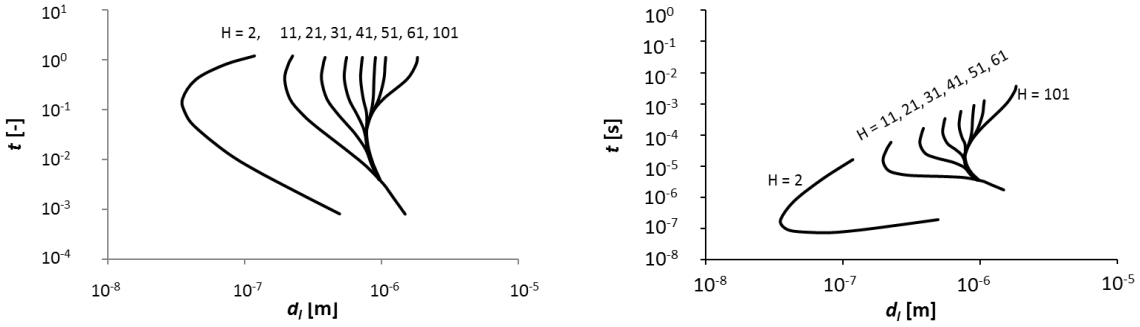

FIG. 4. The critical curves for $H = 2$, 11, 21, 31, 41, 51, 61 and 101 at an initial ethanol mass fraction of $c_b = 0.1$ in the liquid and $c_{t1} = c_{t2} = 0$ in the gas, for dimensionless (left) and dimensional (right) times.

In the next section, these results are analyzed in more detail. First, we determine the main mechanism responsible for the instability. Then we provide a physical explanation for the two types of TPs that appear in Fig. 4. We also analyze more thoroughly the meaning behind the lower parts of the marginal curves of Fig. 4 corresponding to sufficiently small t. Finally, we compare these results with those presented previously in[19] and emphasize the large influence that the gas-phase transients can have on the instability in these situations.

IV. DISCUSSION

A. Instability mechanism

In this subsection, we discuss the relative role of various physical mechanisms that may be responsible for the instability. In[19], it was already shown in a similar physical situation that the solutal Marangoni effect was by far the most important destabilizing mechanism as far as the instability thresholds are concerned. The influence of the temperature field and of convection in the gas phase was also proven to be insignificant in general. We will now show that this is still the case in our present problem. To do so, the following simplifications are introduced into the general formulation. First, the effect of buoyancy (Rayleigh mechanisms)

is not taken into account. Second, the thermal effects are neglected altogether (including the thermal Marangoni mechanism). Also, since the gas mass fractions of the solvent and solute are small, $c_{g1} << 1$ and $c_{g2} << 1$, actually implying small diffusive Péclet numbers[18], we can neglect convection in the gas phase which is then treated as a purely diffusive medium. The "approximate" mathematical model obtained from these and other assumptions is presented in appendix D for the interested reader. The corresponding linear stability analysis takes the form of a one-layer problem, similar to the standard Pearson's one[2,4], albeit with a nonlinear reference profile (see the previous subsection), the solutal Marangoni instead of the thermal one and an appropriately derived solutal Biot number that proves to be a function of the wavenumber of perturbations[18]:

$$Bi_S(k,H) = \rho D \frac{(1-c_{i,ref,l})K_e + c_{i,ref,l}\delta_M\delta_D p_{sat1}}{\left[1+c_{i,ref,l}\left(\delta_M-1\right)\right]^2 \delta_M^{'} p_t^d} k\coth(k(H-1))$$
$$-\frac{\rho D}{H-1}\left(\left(\frac{c_{i,ref,l}}{1+c_{i,ref,l}(\delta_M-1)}\frac{K_e}{\delta_M^{'}p_t^d}-c_{t1}\right)+\delta_D\left(\frac{1-c_{i,ref,l}}{1+c_{i,ref,l}(\delta_M-1)}\frac{p_{sat1}}{\delta_M^{'}p_t^d}-c_{t2}\right)\right). \quad (1)$$

See appendix D for more details. In Eq. (1), $\rho = \rho_g/\rho_l$ is the ratio of the gas and liquid densities, $D = D_{g2}/D_l$ the ratio of the solute (ethanol) diffusion coefficients in the gas and liquid phases, K_e the Henry coefficient (in pressure units), $\delta_M = M_1/M_2$ the solvent to solute molecular mass ratio, $\delta_D = D_{g1}/D_{g2}$ the solvent to solute diffusion coefficient ratio in the gas phase, p_{sat1} the pure solvent saturation pressure, $\delta_M^{'} = M_a/M_1$ the air to solvent molecular mass ratio and p_t^d the (dimensional) ambient pressure. The subscripts "i" and "ref" refer, respectively, to the liquid-gas interface and the reference state. Note that in (1), the case of a zero ambient humidity considered in the present paper corresponds to $c_{t1} = 0$ and $c_{t2} = 0$. The instability mechanism can be quantified by a solutal Marangoni number, proportional to the liquid-layer thickness and to the corresponding reference state mass fraction difference Δc between the bottom and the surface of the liquid layer and given by

$$Ms^* = \frac{\gamma_C \Delta c d_l}{\mu_l D_l},$$

where $\gamma_C \equiv -\partial\gamma/\partial c_l$ is the rate of change of the surface tension γ with the solute mass fraction in the liquid, while μ_l and D_l are the dynamic viscosity and the diffusion coefficient in the liquid. Note that here the quantities $c_{i,ref,l}$ and Δc are functions of t in accordance with the evolution of the reference profile, but this does not really pose any difficulty in

the framework of the frozen-time analysis carried out for each instant t. The instability threshold and the corresponding critical value of the Marangoni number can be obtained by minimizing, with respect to the wavenumber k, the marginal Marangoni curve $Ms^*(k)$. The result, depending parametrically on t, is subsequently recasted in terms of the liquid-layer thickness d_l and shown in Fig. 5 together with the corresponding result of the complete model for $H = 11$ and $H = 101$.

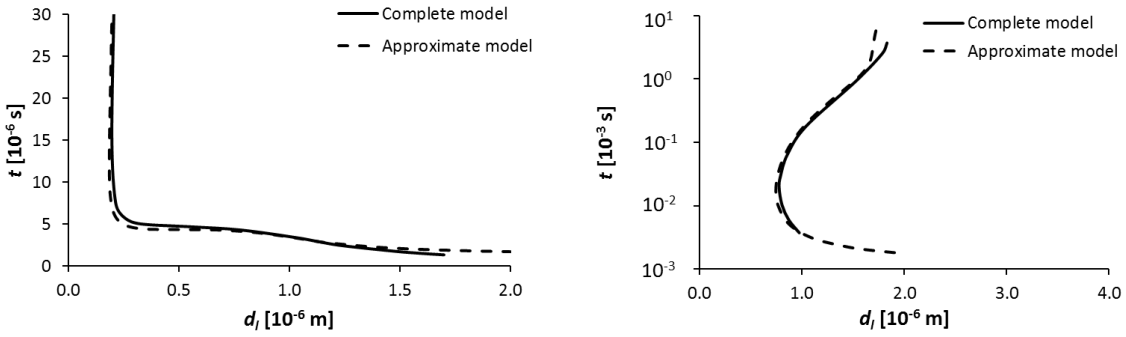

FIG. 5. The critical curves for $H = 11$ (left) and 101 (right) comparing the complete and approximate models ($c_b = 0.1$, $c_{t1} = c_{t2} = 0$).

We observe a good agreement between the complete and the approximate models, even though we cannot guarantee that the difference is entirely due to the neglected effects given the finite precision of the computations. Note also that the curves of Fig. 5 cannot be prolonged to the right more than represented due to the same numerical difficulties. However, their prolongation can be achieved on the basis of a simplified model presented in IV C hereafter. This nevertheless shows that thermal (and thus Soret) and Rayleigh effects can indeed be neglected and that the gas phase can actually be considered as a purely diffusive medium for the vapors. This also confirms that the solutal Marangoni effect is the actual physical mechanism triggering the instability onset. Therefore, the subsequent discussions and physical interpretations will only consider this mechanism. In the next subsections, we will first comment the results corresponding to small values of H. Then, we will present a detailed analysis of the instabilities that can appear at very small times, just after evaporation has begun.

B. Behavior at relatively small H values

From the general observations in section III, we have noticed that there are two types of TPs in Fig. 4 describing the stability results. From a physical point of view, a TP defines a limit thickness below which no instability is ever possible. We have also remarked that the first type of TP appears only for sufficiently small H and the second one for larger values of H, whilst both eventually appear in a narrow intermediate range.

We begin here by analyzing the first type of TP. Table I shows the (dimensionless) time t_{TP1} corresponding to this TP, as a function of H. As mentioned above, this TP appears only for sufficiently small H, when a quasi-stationary behavior is rapidly established in the gas. As argued in subsection III A, it is this quasi-stationarity that is responsible for a distinct maximum of Δc. It is then evident that the system must be most unstable at the times near $t_{\Delta c,max}$, which is confirmed by the fact that $t_{TP1} \approx t_{\Delta c,max}$ in accordance with Table I. This clarifies the nature of the first TP, associated with the maximum of Δc. Note also that the TP appreciably moves as H is changed and disappears approximately together with the maximum of the overall mass-fraction difference in Fig. 3 for H close to 46.

C. Behavior at small times

The second TP, which appears in Fig. 4 for H larger than about 46 and which is independent of H, has a completely different nature. Relatively large values of H and the independence of the second TP from H suggest that it corresponds to a moment when the reference profiles in the gas phase are still essentially transient and not yet quasi-stationary (in other words, the top of the gas layer is not yet reached by the boundary layer developing from the interface). On the other hand, as shown in Table I, the dimensionless values of time (non-dimensionalized with the scale d_l^2/D_l) at the second TP are small, which signals that the liquid boundary layer has not yet quite reached the bottom either. To describe this turning point and to present other physical results, we shall analyze in some detail the solutions of the stability problem corresponding to small times, i.e. to the moments for which the evolving boundary layers in the gas and in the liquid are still far from the limits of the system. These moments are defined by the condition $t << t_{ST}$, where t_{ST} is the smallest of the three diffusion times d_l^2/D_l, $(H-1)^2 d_l^2/D_{g2}$ and $(H-1)^2 d_l^2/D_{g1}$ (ethanol diffusion

times in the liquid and in the gas, and water diffusion time in the gas, respectively). When $H < (1 + \sqrt{D\delta_D}) \approx 160$, one has $t_{ST} = (H-1)^2 d_l^2/D_{g1}$ (water diffusion time in the gas), while $t_{ST} = d_l^2/D_l$ (ethanol diffusion time in the liquid) for larger H values. Fig. 6 is a plot of t_{ST} as a function of d_l, and for several H values, superposed with the earlier obtained marginal-stability results. In what follows, we analyze in detail the stability results that, for a given H, appear in this figure sufficiently below the corresponding dashed straight line t_{ST}.

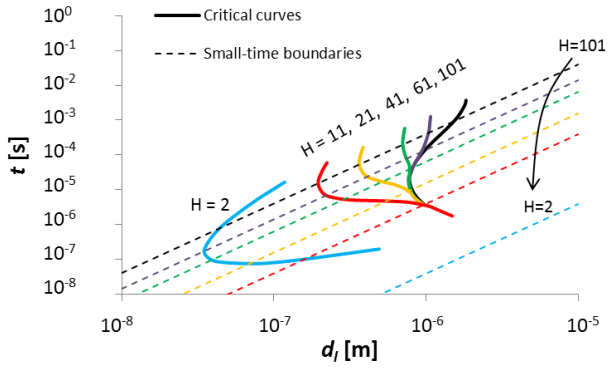

FIG. 6. Results of Fig 4 superimposed with the small-time boundaries t_{ST} for a number of H values.

For the small-time analysis, it is useful to change the length scale used in the non-dimensionalization: instead of d_l, we shall from now on use the penetration depth $\sqrt{D_l t^d}$ of the boundary layer in the liquid as the length scale. To avoid confusion, here we use the supercript "d" for a *dimensional* time variable. Even though the new length scale changes with time, there are actually no implications in the context of the frozen-time approach. Moreover, since only small times are considered, this length scale is actually much smaller than d_l and the dimensionless thickness of the liquid layer $\delta \equiv d_l/\sqrt{D_l t^d}$ is large. Similarly, the dimensionless total height of the system $\widetilde{H} \equiv (d_l + d_g)/\sqrt{D_l t^d}$ is large as well. Using this new length scale in the approximate, one-layer approach introduced in subsection IV A, the appropriate Biot number is $Bi_S(\tilde{k}, \widetilde{H})$ as obtained from Eq. (1). Hereafter the tilde marks the variables pertaining to consideration in the new length scale. Now given that $\widetilde{H} >> 1$ for sufficiently small t^d, whereas one is never interested in too small $\tilde{k}$ (to be discussed later on), the expression for the Biot number simplifies to $\alpha_{Bi}\tilde{k}$, where

$$\alpha_{Bi} = \frac{1}{\tilde{k}} lim_{\tilde{H}\to\infty} Bi_S(\tilde{k}, \tilde{H}) = \rho D \frac{(1 - c_{i,ref,l})K_e + c_{i,ref,l}\delta_D \delta_M p_{sat1}}{\left[1 + c_{i,ref,l}(\delta_M - 1)\right]^2 \delta'_M p_t^d}.$$

Given the Biot number, an approximate expression for the Marangoni number valid for small times can then be obtained as follows. Since the boundary layer remains very thin with respect to the liquid thickness, the reference solution at small times can be approximated by standard self-similar solutions whose closed-form expression is well known (see appendix E). In[28], an equivalent expression for the reference profile is used. However, for the stability analysis, the Biot number in[28] was not dependent on the wavenumber. Using the self-similar solutions for the reference profiles, an analytical expression for the marginal curve in terms of the Marangoni number $\widetilde{Ms^*}$ as a function of $\tilde{k}$ can be deduced much as in the original Pearson problem with a linear reference profile[2,4] (see appendix E for some details):

$$\begin{aligned}
&\widetilde{Ms^*} = \left(4\sqrt{\pi}e^{3\tilde{k}\delta}\left(\alpha_{Bi}\cosh[\tilde{k}\delta]+\sinh[\tilde{k}\delta]\right)\left(-2\tilde{k}\delta+\sinh[2\tilde{k}\delta]\right)\right)\times\\
&\left(\left(-1+e^{2\tilde{k}\delta}\right)\left(-1+e^{4\tilde{k}\delta}-4\tilde{k}\delta e^{2\tilde{k}\delta-\frac{\delta^2}{4}}\right)+\right.\\
&\tilde{k}\sqrt{\pi}\left(-e^{4\tilde{k}^2}\left(2+e^{2\tilde{k}\delta}\left(-2+4\tilde{k}\delta-\delta^2\right)\right)\operatorname{erf}\left[2\tilde{k}-\frac{\delta}{2}\right]\right)+\\
&\tilde{k}\sqrt{\pi}\left(e^{4\tilde{k}(\tilde{k}+\delta)}\left(2-2e^{2\tilde{k}\delta}+4\tilde{k}\delta+\delta^2\right)\operatorname{erf}\left[2\tilde{k}+\frac{\delta}{2}\right]-\delta^2e^{2\tilde{k}\delta}\left(-1+e^{2\tilde{k}\delta}\right)\operatorname{erf}\left[\frac{\delta}{2}\right]\right)-\\
&\left.2\tilde{k}\sqrt{\pi}e^{\tilde{k}(4\tilde{k}+3\delta)}\operatorname{erf}[2\tilde{k}]\left(\left(2+\delta^2\right)\cosh[\tilde{k}\delta]-2\cosh[3\tilde{k}\delta]+4\tilde{k}\delta\sinh[\tilde{k}\delta]\right)\right)^{-1}. \qquad (2)
\end{aligned}$$

Note that boundary conditions have here been expressed at the bottom boundary, as can be guessed by the fact that Eq. 2 depends on δ. For each δ, the critical Marangoni number can be determined by numerically minimizing (2) with respect to $\tilde{k}$. The corresponding results are presented in Fig. 7, where the critical Marangoni number $\widetilde{Ms^*}_{cr}(\delta)$ and the corresponding critical wavenumber are plotted as functions of δ^{-1}. To assess its validity, we have also compared the small-time solution with the (completely numerical) solutions of the approximate model and of the complete model. This comparison is presented in Fig. 8 and shows a very good agreement for small times between the three solutions. For the complete and approximate model, we have considered $H = 101$. To actually determine the critical time corresponding to a given d_l using the small-time approach, the equation $\widetilde{Ms^*}_{cr} = \widetilde{Ms^*}$ is (numerically) solved for δ, where the actual Marangoni number $\widetilde{Ms^*}$ is given by

$$\widetilde{Ms^*} = \frac{\gamma_C\sqrt{D_l t^d}\Delta c}{D_l\mu_l} = \frac{\gamma_C\Delta c}{D_l\mu_l}\frac{d_l}{\delta}, \qquad (3)$$

and shown in Fig. 7 as a function of δ for a number of d_l values. Here $\Delta c \approx 0.0021$ (constant for small times, see subsection III A) in the water-ethanol case with $c_b = 0.1$. Then, knowing $\delta = d_l/\sqrt{D_l t^d}$ and d_l, the critical time can easily be determined.

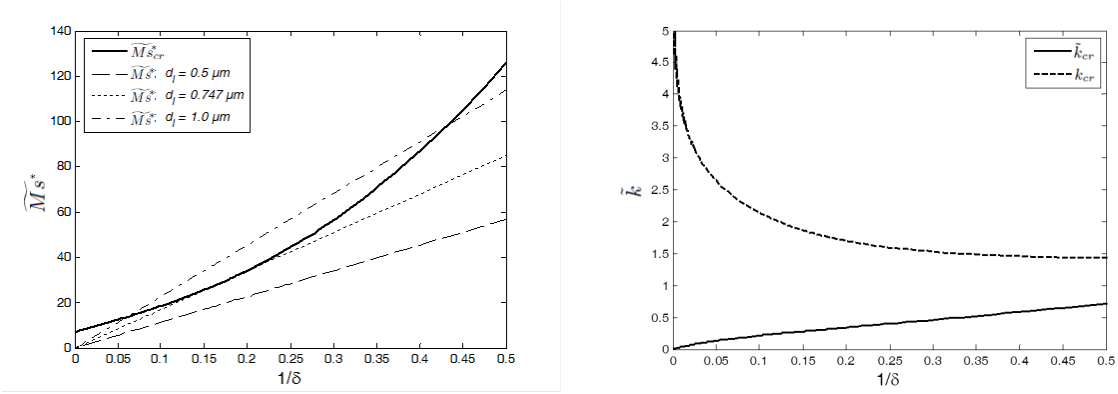

FIG. 7. The critical Marangoni number as a function of $1/\delta$ and the same for the actual Marangoni number at three liquid thicknesses (0.5, 0.747 and 1.0 μm) (left), and the critical wavenumber (both $\tilde{k}_{cr}$ and $k_{cr} = \tilde{k}_{cr}\delta$ in the original scaling) as a function of $1/\delta$ (right) for $c_b = 0.1$ and $c_{t1} = c_{t2} = 0$.

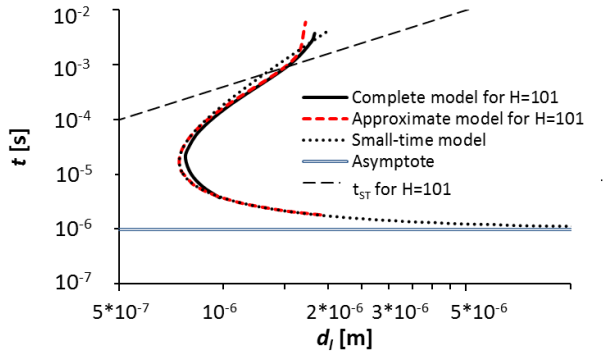

FIG. 8. The critical curve according to various models ($c_b = 0.1, c_{t1} = c_{t2} = 0$).

As far as the critical wavenumber is concerned, let us mention that $\tilde{k}_{cr} \to 0$ as $\delta \to \infty$ in the scaling of the boundary layer, vanishingly thin as compared to the liquid-layer thickness, but the corresponding k_{cr} tends to infinity. This implies that the quantity $\tilde{k}_{cr}\tilde{H}$ ($= k_{cr}H \to \infty$) is large as $t \to 0$, which justifies the earlier made simplification of the expression for the Biot number to $Bi_S = \alpha_{Bi}\tilde{k}$. It is valid in the present context and the stability results for small times are independent of the gas layer thickness, which can be formally considered as infinite.

It is also interesting to note that solutions of the equation $\widetilde{Ms^*}_{cr} = \widetilde{Ms^*}$ for δ cease to exist for sufficiently small d_l. Indeed, as a function of δ^{-1}, the actual Marangoni number is a straight line, whose slope is proportional to d_l. For large enough values of d_l, this straight line intersects the critical Marangoni number curve. The values of $\delta^{-1} = \sqrt{D_l t^d}/d_l$ at the intersections define of course the critical times for this given d_l that can be observed in Fig. 8. For smaller values of d_l, there is no intersection between the marginal curve and the straight line. This means that for sufficiently small d_l, the system is always stable. The critical value of the liquid thickness, for which the actual Marangoni number is just tangent to the critical curve in Fig. 7, corresponds in fact to the turning point in Fig. 8, here with $d_l = 0.747$ μm. One can then propose the following interpretation of this TP. On the one hand, the liquid mass fraction boundary layer grows with time ($\delta^{-1} \uparrow$), which destabilizes the reference solution (indeed, the actual Marangoni number (3) increases proportionally to δ^{-1}). On the other hand, the perturbations which develop have a penetration depth which also grows with time, hence they become more efficiently dissipated by viscous friction and mass diffusion at the bottom plate (the critical Marangoni number increases more than proportionally with δ^{-1}). Whether or not instability sets in therefore depends on the competition between these two effects, which turns in favor of the former above a certain critical value of the liquid thickness (corresponding to the turning point).

As a final remark on Fig. 7, let us mention that the latter shows that the critical time of the instability onset is a decreasing function of d_l (see also Fig. 8). After showing above that there exists a certain limiting value of d_l below which no instability ever occurs, we shall now prove that there exists also a limiting time before which the system remains stable whatever the value of d_l. To do so, we shall analyze the behavior of the system as $d_l \to \infty$, which amounts to considering the limit $\delta \to \infty$. Applying this to Eq. (2) yields

$$\widetilde{Ms^*} = \frac{(1+\alpha_{Bi})\sqrt{\pi}}{1 - 2\tilde{k}\sqrt{\pi}e^{4\tilde{k}^2}\mathrm{erfc}(2\tilde{k})}. \tag{4}$$

The minimum of this expression with respect to the wavenumber corresponds to $\tilde{k} = 0$ and yields the critical Marangoni number

$$\widetilde{Ms^*}_{cr,d_l\to\infty} = (1+\alpha_{Bi})\sqrt{\pi} = \left(1 + \rho D \frac{(1-c_{i,ref,l})K_e + c_{i,ref,l}\delta_D\delta_M p_{sat1}}{\left[1 + c_{i,ref,l}(\delta_M - 1)\right]^2 \delta'_M p_t^d}\right)\sqrt{\pi}. \tag{5}$$

Making the actual Marangoni number (3) equal to the one above allows to determine the asymptotic value of the critical time

$$t^d_{cr,d_l\to\infty} = \frac{1}{D_l}\left(\frac{D_l\mu_l}{\Delta c\gamma_C}\left(1+\rho D\frac{(1-c_{i,ref,l})K_e + c_{i,ref,l}\delta_D\delta_M p_{sat1}}{\left[1+c_{i,ref,l}(\delta_M-1)\right]^2\delta'_M p^d_t}\right)\sqrt{\pi}\right)^2. \qquad (6)$$

With the previously calculated value for $c_{i,ref,l} = c_b - \Delta c$ (where $c_b = 0.1$ and $\Delta c \approx 0.0021$), one obtains $\widetilde{Ms^*}_{cr,d_l\to\infty} \approx 7.11$ and $t^d_{cr,d_l\to\infty} \approx 9.82 * 10^{-7}s$ ($\approx 1\mu s$). The corresponding asymptote is indicated in Fig. 8. Note that while the general form of the expression (2) and the corresponding TP consideration make sense only for sufficiently large H ($H > 46$, see above), the results (4)-(6) are actually valid in the asymptotic sense for no matter what value of $H = O(1)$.

D. The importance of transients in the gas phase

In the present analysis of evaporative instabilities in a binary liquid, the transients of the reference state, and importantly those in the gas, are considered in full. In the previous work[19], only the ethanol mass fraction profile in the liquid phase was considered as transient, whilst all other profiles (temperatures and mass fractions in the gas) were assumed quasi-stationary and "slaved" to the time variations of the liquid ethanol mass fraction. This model will be called here the "partially transient model", while the model of the present paper will be referred to as the "complete" model to avoid ambiguity. It is the purpose of the present subsection to compare the two models.

Fig. 9 presents the comparison of the critical curves (again in the plane t versus d_l) between the complete and the partially transient models for the values of H previously considered in this paper. Note that for completeness, the asymptote described previously and the results of the "approximate" fully transient model described in IV A are also incorporated into the figure. Besides, the time t_{ST} (the smallest of the characteristic diffusion times, as discussed earlier) is shown. This time can be used as well to distinguish qualitatively the boundary between the self-similar description and the quasi-stationary state in the gas (for the H values considered). We can notice that, for each H, the partially transient and complete models correspond well with each other "sufficiently above" the t_{ST} lines (keeping in mind that the upper branch of the figure corresponds to the system getting back to

stability if the reference solutions had not been perturbed earlier). In particular, the first type of TP (discussed in section IV B) is correctly described by both models. Of course, it is because the instability occurs in the system after quasi-stationarity is reached in the gas that the results of the partially transient model agree well with those of the complete approach. On the contrary, when the complete model predicts an instability before the gas has become quasi-stationary, the results of the partially transient model are incorrect and in particular, the second TP (discussed in section IV C) is not present in this latter approach.

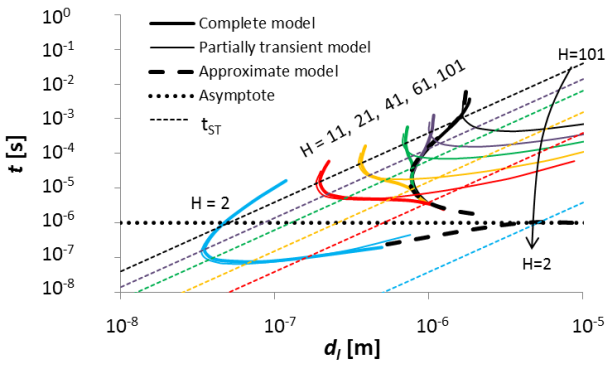

FIG. 9. Critical curves for various H values, comparing the complete and the partially transient models ($c_b = 0.1$, $c_{t1} = c_{t2} = 0$).

V. CONCLUSIONS

The present paper has been concerned with the analysis of Bénard instabilities in a layer of an aqueous solution of ethanol undergoing evaporation into air, including transient reference profiles following initial contact between both phases. The discussion was first focused on mass-fraction reference profile in both the liquid and the gas phases, since it appeared that their development bore much more importance on the instability onset than the temperature profiles. The evaporation process expressed in terms of the mass-fraction profiles subdivides into four stages. The first one starts with a sudden mass-fraction jump at the interface at $t = 0$, typical when putting into contact two homogeneous out-of-equilibrium media (the liquid and the gas). This first stage continues in a self-similar solution, where the mass fractions at the interface stay constant and the mass-fraction profiles start to penetrate both in the liquid and in the gas phases. As soon as the gas mass fraction attains a quasi-stationary state by reaching the top boundary, the mass fractions at the interface begin to

decrease, the system entering the second stage. The third stage is characterized by the liquid mass-fraction boundary layer attaining the bottom of the liquid, and the depletion of the (most volatile) solute at the bottom begins. Finally, a fourth stage has been identified, where the liquid mass fraction profile hardly changes its form. In other words, the depletion occurs at a nearly constant rate. It should be noted, though, that for large H values, the third stage occurs earlier than the second stage. These successive stages correspond to different evolutions of the overall mass-fraction difference across the liquid layer. During the first (self-similar) stage, this difference is constant. Then, if the quasi-stationarity in the gas is attained earlier than the liquid mass-fraction boundary layer reaches the bottom (i.e. in the second stage), the overall mass-fraction difference increases. After the liquid mass fraction has reached the bottom (third stage), considering a certain delay in order to catch up with the mass-fraction decrease at the interface, the overall mass fraction difference decreases again. On the contrary, when the liquid mass fraction attains the bottom earlier than quasi-stationarity is reached in the gas (i.e. third stage occurs earlier than the second one, i.e. for large H), a monotonic decrease is observed and no maximum overall mass-fraction difference occurs. These stages are important when analyzing the instability behavior.

First of all, it has been determined that in this paper too (referencing to the previous papers[18,19]), the solutal Marangoni mechanism is the main one responsible for triggering the instability and a number of other effects accounted for in the full model turn out to be inessential. This has been shown by using an approximate model (along the lines of a Pearson-like model, albeit with nonlinear reference profiles and a wavenumber-dependent solutal Biot number), taking into account only the solutal Marangoni effect and implementing simplifications related to the inessential effects. The results agreed well with those of the complete model. As such, in the discussions, the solutal Marangoni mechanism is the only one used for understanding the results.

Critical curves have been drawn yielding the time for the onset of instabiliy (in the frozen-time sense) versus the liquid-layer thickness. This has been done for several H values. For all H values, a certain critical liquid thickness has been identified (named the turning point), below which no instability occurs at all times. For small H values, it has been observed that this turning point occurs circa the moment the overall mass-fraction difference across the liquid layer is at its maximum (cf. the above discussion for the reference profiles). For large H values, a different type of turning point emerges (and actually for intermediate values

of H, both turning points eventually coexist), having a different behavior with respect to variations of H, because it is induced by different physical mechanisms. Namely, it was noted that it corresponds to relatively small times, that is to the early stage of the evaporation process, before the gas reaches quasi-stationarity and the liquid mass-fraction boundary layer reaches the bottom. For the reference profiles this means that a self-similar approach can be used, determining thereby the mass fraction jump at the interface. Although the turning point occurs when the reference-profile boundary layers are still far from the bottom and top boundaries, the perturbations start nonetheless sensing the bottom of the liquid, which is what is actually responsible for the occurrence of this turning point. This was confirmed by obtaining a closed-form analytical expression for the marginal Marangoni curve and comparing successfully the resulting critical conditions with the results of the complete model for large H values. It is also worth stressing that this turning point proves to be independent of the gas-layer thickness. Indeed, the boundary layer in the gas is still sufficiently close to the interface when the instability sets in and the gas layer can thus be considered as semi-infinite at this moment, whatever its actual height.

Another important aspect considered in the present paper concerns the critical time before which the system remains always stable. It appears that as the liquid layer thickness is increased the time for the instability onset approaches a certain asymptotic value independent of H. This can be understood by the observation that for very large thicknesses the boundary layers in the liquid and gas phases are too far from respectively the bottom and top boundaries for the former ones to sense the latter ones. The small-time application of the model of the present paper has been used in order to determine the value of this asymptotic time, being of the order of $1\mu s$ for the 10 %wt solution of ethanol in water.

Finally, the results of the fully transient model of the present paper were compared to the partially transient model, which assumes quasi-steady mass fraction profiles in the gas phase[19]. The analysis performed here has evidenced that the instability onset can occur at (much) smaller times and for (much) smaller critical thicknesses than predicted under the assumption of quasi-steadiness in the gas. This seems to be an attribute of a "very unstable" system, for which the instability can occur before quasi-stationarity sets in in the gas. Since this decrease of instability thresholds is not predicted by the partially transient model, it is a direct consequence of the transients in the gas phase. Physically, such destabilization owes itself to larger concentration gradients (and consequently larger evaporation fluxes)

occurring for the reference profile in the gas at the initial, self-similar stage as compared to the later, quasi-stationary stage.

ACKNOWLEDGEMENTS

The authors acknowledge the financial support of the European Space Agency and of the Belgian Science Policy through the PRODEX projects. P.C. also acknowledges the financial support of the Fonds de la Recherche Scientifique (FNRS).

REFERENCES

[1]H. Bénard, "Les tourbillons cellulaires dans une nappe liquide transportant de la chaleur en régime permanent," Ann. Chem. Phys. **23**, 62 (1901)

[2]J.R.A. Pearson, "On convection cells induced by surface tension," J. Fluid Mech. **4**, 489 (1958)

[3]C. Normand, Y. Pomeau, M. Velarde, "Convective instability: a physicist's approach," Rev. Mod. Phys. **49**, 581 (1977)

[4]P. Colinet, J.C. Legros, M.G. Velarde, *Nonlinear Dynamics of Surface Tension Driven Instabilities* (Wiley-VCH Verlag GmbH, Berlin, 2001)

[5]B. Haut, P. Colinet, "Surface-tension-driven instabilities of a pure liquid layer evaporating into an inert gas," J. Colloid Interface Sci. **285**, 296 (2005)

[6]J. Margerit, M. Dondlinger, P.C. Dauby, "Improved 1.5-sided model for the weakly nonlinear study of Bénard-Marangoni instabilities in an evaporating liquid layer," J. Coll. Interf. Sc. **290**, 220 (2005)

[7]K.E. Uguz, R. Narayanan, "Instability in evaporative binary mixtures. I. The effect of solutal Marangoni convection," Phys. Fluids **24**, 094101 (2004)

[8]K.E. Uguz, R. Narayanan, "Instability in evaporative binary mixtures. II. The effect of Rayleigh convection," Phys. Fluids **24**, 094102 (2004)

[9]V.-M. Ha, C.-L. Lai, "Onset of Marangoni instability of a two-component evaporating droplet," Int. J. Heat Mass Transfer **45**, 5143 (2002)

[10]P.G. de Gennes, "Instabilities during the evaporation of a film: Non-glassy polymer + volatile solvent," Eur. Phys. J. E. **6**, 421 (2001)

[11]F. Doumenc, T. Boeck, B. Guerrier, M. Rossi, "Transient Rayleigh-Bénard-Marangoni convection due to evaporation: a linear non-normal stability analysis," J. Fluid Mech. **648**, 521 (2010)

[12]B. Trouette, E. Chénier, F. Doumenc, C. Delcarte, B. Guerrier, "Transient Rayleigh-Bénard-Marangoni solutal convection," Phys. Fluids **24**, 074108 (2012)

[13]S. Serpetsi, S. Yiantsios, "Stability characteristics of solutocapillary Marangoni motion in evaporating thin films," Phys. Fluids 24, 122104 (2012)

[14]N. Kurenkova, K. Eckert, E. Zienicke, A. Thess, "Desorption-driven convection in aequous alcohol solution," Lect. Notes Phys. **628**, 403 (2003)

[15]J. Zhang, A. Oron, R. Behringer, "Novel pattern forming states for Marangoni convection in volatile binary liquids," Phys. Fluids **23**, 072102 (2011)

[16]G. Toussaint, H. Bodiguel, F. Doumenc, B. Guerrier, C. Allain, "Experimental characterization of buoyancy and surface tension driven convection during the drying of a polymer solution," Int. J. Heat Mass Transfer **51**, 4228 (2008)

[17]S. Dehaeck, C. Wylock, P. Colinet, "Evaporating cocktails," Phys. Fluids **21**, 091108 (2009)

[18]H. Machrafi, A. Rednikov, P. Colinet, P.C. Dauby, "Bénard instabilities in a binary-liquid layer evaporating into an inert gas," J. Colloid Interface Sci. **349**, 331 (2010)

[19]H. Machrafi, A. Rednikov, P. Colinet, P.C. Dauby, "Bénard instabilities in a binary-liquid layer evaporating into an inert gas: stability of quasi-stationary and time-dependent reference profiles," Europ. Phys. J. S.T. **192**, 71 (2011)

[20]See supplementary material at [URL will be inserted by AIP] for the appendices

[21]M. Dondlinger, P. Colinet, P.C. Dauby, "Influence of a nonlinear reference temperature profile on oscillatory Bénard-Marangoni convection," Phys. Rev. E **68**, 066310 (2003)

[22]G.J.M. Pieters, C.J. van Duijn, "Transient growth in linearly stable gravity-driven flow in porous media," Eur. J. Mech. B/Fluids **25**, 83 (2006)

[23]L. Czechowski, K. Kossacki, "Thermal convection in the porous methane-soaked regolith of Titan: Investigation of stability," Icarus **202**, 599 (2009)

[24]P.C. Dauby, G. Lebon, "Bénard-Marangoni instability in rigid rectangular containers," J. Fluid Mech. **329**, 25 (1996)

[25]P.C. Dauby, G. Lebon, E. Bouhy, "Linear Bénard-Marangoni instability in rigid circular containers," Phys. Rev. E **56**, 520 (1997)

[26]R. Liu, Q.S. Liu, S.C. Zhao, "Influence of Rayleigh effect combined with Marangoni effect on the onset of convection in a liquid layer overlying a porous layer," Int. J. Heat Mass Transfer **51**, 6328 (2008)

[27]C. Canuto, M.Y. Hussaini, A. Quarteroni, T.A. Zang, *Spectral methods in fluid dynamics* (Springer, New York, 1988)

[28]Z.F. Sun, "Onset of Rayleigh-Bénard-Marangoni convection with time-dependent nonlinear concentration profiles," Chem. Eng. Science **68**, 579 (2012)